In Search of the Smallest Boroxol-Type Heterocyclic Ring System: Planar Hexagonal $B_3S_3^+$ Cluster with Double $6\pi/2\sigma$ Aromaticity

Li-Juan Zhang,‡[a] Lin-Yan Feng,‡[b] He Bian,[a] Ling Pei,[a] Da-Zhi Li*[a] and Hua-Jin Zhai*[b]

[a]*College of Chemistry and Chemical Engineering, Binzhou University, Binzhou 256603, Shandong, China*

[b]*Nanocluster Laboratory, Institute of Molecular Science, Shanxi University, Taiyuan 030006, China*

E-mail: ldz005@126.com (D.-Z.L.); hj.zhai@sxu.edu.cn (H.-J.Z.)

‡ L.-J. Zhang and L.-Y. Feng contributed equally to this work.

Abstract

Boroxol (B_3O_3) rings and relevant hexagonal B_3S_3 structural blocks are ubiquitous in boron oxide/sulfide glasses, crystals, and high temperature liquids. However, the isolation of an ultimate heterocyclic B_3O_3 or B_3S_3 cluster in the free-standing form, with as few as six atoms, has been unsuccessful so far. We report on computational design of the simplest case of such a system: highly symmetric D_{3h} $B_3S_3^+$ ($^1A_1'$) cluster. It is the well-defined global minimum on the potential energy surface, following global searches and electronic structure calculations at the B3LYP and single-point CCSD(T) levels. Chemical bonding analysis reveals an ideal system with skeleton Lewis B–S σ single bonds and unique double 6π/2σ aromaticity, which underlies its stability. The cluster turns out to be an inorganic analog of the 3,5-dehydrophenyl cation, a typical double π/σ aromatic system. It offers an example for chemical analogy between boron-based heterocyclic clusters and aromatic hydrocarbons. Double π/σ aromaticity is also a new concept in heterocyclic boron clusters. Prior systems such as borazine, boroxine, and boronyl boroxine only deal with π aromaticity as in benzene.

Keywords: boron sulfide clusters; boron-based heterocyclic clusters; boroxol ring; chemical bonding; double π/σ aromaticity.

1. Introduction

The intrinsic electron-deficiency of elemental boron leads to its rich chemistry. Boron-based nanoclusters show unique structural and electronic properties, as well as novel chemical bonding governed by π/σ aromaticity, antiaromaticity, and conflicting aromaticity.[1–17] Anion boron clusters were characterized to assume planar or quasi-planar (2D) geometries in a wide range of sizes up to 40 atoms,[9,15] which feature triangular close-packing 2D structures that are decorated by defect holes. Borospherenes[15,18–20] were observed as "cubic cages" with interwoven boron double chains, whose surfaces have hexagonal versus heptagonal holes. Boron double chains were also observed as structural blocks in tubular boron clusters[8] and extended 2D boron materials such as borophenes.[21,22] Defect holes (including hexagonal holes) in low-dimensional boron systems help compensate for their electron-deficiency. For the same reason, monocyclic rings or single chains are nonexistent in bare B clusters, in contrast to carbon.[23] Chemical analogy has been established systematically in recent years between boron clusters and hydrocarbons.[9,24,25]

Intuitively, oxidation or sulfuration of boron clusters results in boron oxide or sulfide clusters,[26] which should be even more electron-deficient because such processes withdraw electrons from boron. Nonetheless, binary B–O/B–S clusters can form heterocyclic structures and make use of O 2p or S 3p lone-pairs for π delocalization, allowing new types of chemical bonding.[26–36] A variety of B–O clusters were reported lately, demonstrating the key role of boronyl (BO) group[24] as a new inorganic ligand, which parallels CN or CO. In the B–O clusters, heteroatomic rhombic, pentagonal, and hexagonal rings were found to be crucial structural cores. Rhombic B–O clusters led to the discovery of a new type of four-center four-electron (4c-4e) π bond: the "o-bond".[26,31] Hexagonal B–O clusters succeeded in introducing new members[30,33,36] to the so-called "inorganic benzene" family, following borazine and boroxine. In comparison to oxides, boron sulfide clusters have received limited attention in the literature, although S and O are closely similar in valence configurations.

Selected literature on binary B_mS_n clusters are surveyed here. In the 1960s and 1970s, mass

spectroscopic studies in the gas phase confirmed the existence of a series of boron sulfide cations, suggesting that BS_2^+, $B_2S_2^+$, and $B_2S_3^+$ are important precursors to form high molecular weight B–S clusters.[37–41] Quite recently, computational works from us revealed rhombic B_2S_2 and pentagonal B_3S_2 rings in the B_4S_4 and $B_3S_2H_3$ clusters, respectively.[42–44] The D_{2h} $B_6S_6^{0/-/2-}$ global-minimum (GM) clusters[45] were found to contain fused twin B_3S_2 rings with elongated overall shapes. A series of simple B–S clusters, BS_n^- (n = 1–3) and BSO^-, were experimentally characterized using photoelectron spectroscopy (PES).[46,47] In terms of bonding, rhombic B_4S_4 cluster[42] features an o-bond. Pentagonal heterocyclic B–S clusters[44] have 4π electrons and naturally extend the o-bond concept, which is called a pentagonal o-bond. The latter is π aromatic despite its 4π electron-counting. Relevant pentagonal 5π systems can be considered inorganic analogs of cyclopentadiene. Such an analogy may be further extended to polycyclic aromatic hydrocarbons (PAHs).[45]

Among boron-based B–O/B–S heterocyclic structures, boroxol (B_3O_3) ring appears to dominate the glassy bulk B_2O_3 and high temperature B_2O_3 liquids, probably constituting a large fraction up to 75% in the former case.[48] However, these boroxol rings are interlinked in a truly 3D fashion. Our attempts to isolate a boroxol ring in free-standing $B_3O_3^{+/0/-}$ clusters turned out to be a failure.[31] The B–O clusters were shown to stabilize a boroxol ring, only upon attachment of extra ligands.[30,33,34,36] Such clusters include D_{3h} B_6O_6 (boronyl boroxine), C_{2v} $B_5O_5^{+/0}$, C_s $B_4O_5^-$, and down in size to C_s $B_4O_4^+$, which are extremely sensitive to charge states and every atom or electron makes a difference. Given the importance of boroxol ring in boron oxide materials, some fundamental questions remain open. What is the smallest cluster that can possibly stabilize a B_3O_3 ring (or its B_3S_3 counterpart)? Is a B_3O_3 or B_3S_3 ring cluster with six atoms viable in the free-standing form? If not, why? What is the possible charge state in order to make a B_3O_3 or B_3S_3 ring stable? How does a B_3S_3 ring differ from B_3O_3 in physical chemistry?

To achieve the above goal, the only option left to date is to thoroughly explore the title $B_3S_3^+$ system, because all $B_3O_3^{+/0/-}$ and $B_3S_3^{0/-}$ species do not form hexagonal rings.[31,43] In bulk B_2S_3 crystals,[49] hexagonal B_3S_3 and rhombic B_2S_2 rings are linked via S bridges to form almost

planar infinite 2D high-polymer layers, hinting that heterocyclic B_3S_3 rings are probably more isolable with respect to their B_3O_3 counterparts in glassy bulk B_2O_3 or high temperature B_2O_3 liquids. Indeed, our present work shows that the $B_3S_3^+$ cluster possesses a hexagon-type GM structure with extra (albeit relatively weak) B–B–B bonding so that it has a triangular overall shape, a distorted version of heteroatomic hexagon. The D_{3h} $B_3S_3^+$ GM cluster is the ultimate lower bound for a boroxol-type system, which turns out to be energetically well-defined and structurally elegant. In terms of chemical bonding, D_{3h} $B_3S_3^+$ GM cluster features 6π plus 2σ double aromaticity, which is an inorganic analog of 3,5-dehydrophenyl cation $C_6H_3^+$ (D_{3h}, $^1A_1'$),[50,51] the first designer hydrocarbon with double π/σ aromaticity. Double aromaticity is sort of a new concept in boron-based heterocyclic clusters,[26] because prior systems such as borazine, boroxine, and boronyl boroxine[30] only have π aromaticity. The title cluster also helps deepen our understanding on the binary B–O and B–S systems, suggesting intriguing opportunities for novel B–S clusters in forthcoming studies.

2. Methods

Computer global searches for the $B_3S_3^+$ system were performed with density functional theory (DFT) at the hybrid B3LYP/3-21G level, using the Coalescence Kick (CK) algorithm.[52−54] The effort was aided with manual structural constructions. For the title cluster with as few as six atoms, the potential energy surface is anticipated to be thoroughly explored in this work and the identification of GM cluster should be conclusive. A total of 1500 stationary points were probed during the CK searches, many of which turned out to be duplicated upon reoptimization at a higher level. Low-lying candidate structures were then fully reoptimized at the B3LYP level[55,56] with the 6-311+G(d,p) basis set, as implemented in the Gaussian 16 package.[57] Vibrational analyses were done at the same level to ensure that the reported structures are true minima.

To check for consistency, relative energies were also calculated using the PBE0 functional with symmetry constraints.[58] The energetics for top eight isomers were further benchmarked

using single-point CCSD(T) calculations[59] at their B3LYP/6-311+G(d,p) geometries, which are considered the ultimate energetics data in this work. The B3LYP and PBE0 methods produced essentially the same geometries for the isomers and only the B3LYP structures will be discussed.

The NBO 5.0 program[60] was used for natural bond orbital (NBO) analysis, which gives the Wiberg bond indices (WBIs) and natural atomic charges. Chemical bonding in $B_3S_3^+$ cluster and its hydrocarbon analog ($C_6H_3^+$) was elucidated using canonical molecular orbital (CMO) analyses and adaptive natural density partitioning (AdNDP).[61] The Multiwfn program[62] was used for orbital composition analyses.

3. Results

3.1. Global-minimum D_{3h} $B_3S_3^+$ cluster and selected isomeric structures

The GM structure of $B_3S_3^+$ cluster, **1** (D_{3h}, $^1A_1'$) as identified from our global searches, is illustrated in Fig. 1(a). Alternative low-lying isomers are shown in Fig. 2. The energetics data at the B3LYP, PBE0, and CCSD(T) levels consistently suggest that cluster **1** is the GM structure, being 1.18 eV more stable than its nearest competitor at single-point CCSD(T) (Fig. 2). Cluster **1** is perfectly planar with a triangular B_3 ring as structural core; three S atoms occupy bridging positions. This type of geometry can be viewed as a variation of heterocyclic hexagon, owing to extra B–B bonding (*vide infra*).

(Figure 1)

The B–S bond distances in cluster **1** are 1.78 Å, which lie in between single (1.88 Å) and double (1.72 Å) bonds,[63] hinting the presence of a delocalized bonding system. Note that typical B=S double and B≡S triple bonds are 1.68 and 1.63 Å, respectively.[46,47] The B–B distances in **1** (1.71 Å) are close to the upper bound for single bond (1.70 Å);[63] a typical B–B single bond such as in D_{3h} B_4O_3 cluster[28] is 1.66 Å. Thus, the B–B links are moderately longer than single bonds. The calculated WBIs for the B–S and B–B links amount to 1.26 and 0.56, respectively (Fig. 1(b); see also Table 1), correlating perfectly with their bond distances.

(Figure 2)

(Table 1)

Among alternative low-lying isomers of the $B_3S_3^+$ system, **2** (C_{2v}, $^1A_1$) and **3** (D_{3h}, $^1A_1'$) are of interest, although they are substantially higher in energy by 1.18 and 3.01 eV with respect to cluster **1** at single-point CCSD(T). Isomer **2** is composed of a distorted B_2S_2 rhombus (1.70/1.92 Å) and a terminal B≡S group (1.60 Å). The average of the former distances are shorter than single bonds, in line with an o-bond system.[26] The B–B link in **2** (1.63 Å) should be a single bond. Isomer **3** has a D_{3h} B_3 core (1.73 Å) and three terminal S atoms (B–S: 1.60 Å). The former distances are comparable to those in **1** and the latter are assigned as the B≡S groups.

3.2. Thermodynamic and kinetic stabilities

Early mass spectroscopic studies suggested that cationic $B_2S_2^+$ cluster may be a precursor for high molecular weight clusters.[40] It is valuable to calculate the formation energy of D_{3h} $B_3S_3^+$ (**1**) cluster using linear $B_2S_2^+$ and BS species as reactants, according to this equation: $B_2S_2^+$ ($D_{\infty h}$, $^2\Sigma_g$) + BS ($D_{\infty h}$, $^2\Sigma_g$) = $B_3S_3^+$ (**1**, D_{3h}, $^1A_1'$). The formation energy evaluated is –126.9 kcal mol^{-1} (–5.50 eV) at the B3LYP/6-311+G(d,p) level, suggesting that the formation of cluster **1** is highly exothermic, which is no surprise.

(Figure 3)

To assess dynamic stability of GM cluster **1**, we did Born-Oppenheimer molecular dynamics (BOMD) simulations[64] at the B3LYP/6-311+G(d,p) level, for 30 ps at the selected temperatures of 300, 500, and 900 K. The calculated root-mean-square deviations (RMSDs) and maximum bond distance deviations (MAXDs) are plotted in Fig. 3. The average RMSDs are quite small (from 0.04 to 0.07 Å), indicating that D_{3h} $B_3S_3^+$ (**1**) cluster has excellent kinetic stabilities, being robust against isomerization and decomposition. Again, the observation is no surprise.

4. Discussion

4.1. Chemical bonding in D_{3h} $B_3S_3^+$ cluster: canonical molecular orbital analysis and

adaptive natural density partitioning (AdNDP)

Chemical bonding dictates cluster structures and the CMO analysis is of fundamental importance in understanding a molecular system. The D_{3h} $B_3S_3^+$ (**1**) cluster has 26 valence electrons. All occupied CMOs are depicted in Fig. 4, sorted to four categories. Subset (c) has three CMOs, which are composed of S 3s atomic orbitals (AOs). The bottom HOMO–8 (HOMO stands for the highest occupied molecular orbital) is an in-phase combination between three S centers, whereas the degenerate HOMO–7/HOMO–7′ pair have one nodal plane. The three CMOs are in bonding/nonbonding/antibonding combination for a triangular system, following the CMO building principles. They can be recombined to recover three S $3s^2$ lone-pairs, one for each S atom. Subset (d) has six CMOs that are composed of B 2p and S 3p AOs, which orient either radially or tangentially with respect to the S_3 triangle. Each and every of these CMOs is primarily responsible for B–S σ bonding along the heterocycle. They are attributed to six Lewis B–S σ single bonds, similar to the skeleton σ bonds in benzene. The above bonding elements collectively consume 18 electrons.

(Figure 4)
(Table 2)

The remaining 8 electrons in cluster **1** form delocalized π/σ frameworks. Subset (b) has three CMOs, following exactly the spatial pattern of π sextet in benzene. At the zeroth order, these π CMOs are derived from three S $3p_z$ lone-pairs. However, owing to high covalency of B–S bonding in **1**, the B $2p_z$ AOs participate heavily in them, by 13.2% in HOMO–1/HOMO–1′ and 46.2% in HOMO (Table 2). Collectively, three B centers contribute 1.5 electrons in π framework, compared to 4.5 electrons from S centers. In short, the π framework is truly six-center in nature, which cannot be transformed to classical Lewis elements. It renders π aromaticity for cluster **1**, according to the $(4n + 2)$ Hückel rule. The delocalized σ framework contains only one CMO: HOMO (Fig. 4(a)). It is perfectly covalent with 46.2% B 2p and 48.6% S 3p contributions, leading to the simplest case of 2σ aromaticity for a hexagonal structure. Intuitively, one can consider that σ aromaticity originates primarily from the B_3 triangle (*vide infra*), because B

centers are unsaturated. Thus, cluster **1** has both π/σ aromaticity with the 6π and 2σ electron-counting, respectively.

(Figure 5)

The above bonding picture can be reproduced *via* AdNDP analysis (see Fig. 5).[61] Here all bonding elements are straightforward and easy to comprehend: three S $3s^2$ lone-pairs, six Lewis B–S σ bonds, π sextet, and 2σ delocalization. All occupation numbers (ONs) are close to ideal. Clearly, cluster **1** is doubly 6π/2σ aromatic as confirmed by the AdNDP data. The delocalized 2σ framework is treated as a 3c-2e B–B–B σ bond, which gives an ON of 1.97 |e|, probably due to recombination of HOMO–6 with HOMO–8. Owing to the triangular rather than hexagonal shape of cluster **1**, the π sextet can be alternatively partitioned as three 3c-2e B–S–B "island" π bonds (Fig. 5(b)). Note that even this island scheme is delocalized, which should not be confused to the Kekulé model of benzene. The two AdNDP π schemes are equivalent and yet the latter shows evidence that the π framework is truly delocalized on a 2D plane (rather than on hexagonal ring only). The consequence is that the calculated WBIs for B–B links are markedly greater than 0.33, whereas those for B–S links are lower than 1.50 (see Fig. 1(b) and Table 1).

4.2. Doubly 6π/2σ aromatic D_{3h} $B_3S_3^+$ cluster as an inorganic analog of 3,5-dehydrophenyl cation

Double π/σ aromaticity are scarce in boron-based heterocyclic hexagonal systems.[26] Indeed, inorganic benzenes (borazine, boroxine, and boronyl boroxine[30]) have saturated B sites via terminal B–H or B–BO σ single bonds, so that only π delocalization is possible. Therefore, the present D_{3h} $B_3S_3^+$ (**1**) cluster with 6π/2σ double aromaticity is an exception. It is reminiscent of the 3,5-dehydrophenyl cation, $C_6H_3^+$ (D_{3h}, $^1A_1'$).[50,51] The latter species is derived from benzene upon removal of three H atoms and one electron, thus introducing a new delocalized σ framework. Overall, D_{3h} $C_6H_3^+$ cluster is doubly 6π/2σ aromatic, which has been routinely cited as a milestone work in aromaticity/antiaromaticity. Its AdNDP bonding scheme is presented in Fig. 6, for the first we believe. The scheme is elegant and clearly demonstrates the nature of

6π/2σ double aromaticity.

(Figure 6)

Both the D_{3h} $B_3S_3^+$ (**1**) and D_{3h} $C_6H_3^+$ clusters assume high D_{3h} ($^1A_1'$) symmetry with a heterocyclic hexagonal shape. They are 26-electron systems, whose AdNDP bonding elements virtually show one-to-one correspondence (Fig. 5 versus Fig. 6). Chemically, three C–H units in D_{3h} $C_6H_3^+$ are equivalent to S centers in **1**, because a terminal C–H σ bond locks a pair of electrons locally, which are no different from a S $3s^2$ lone-pair in terms of bonding in the hexagon. The remaining three C centers correspond to the B sites. The two species differ in that the π sextet in **1** originates from three S $3p_z$ lone-pairs (with about 25% B mixture), while that in D_{3h} $C_6H_3^+$ is uniformly contributed from all six C centers. The 2σ delocalization in two species are quite the same. Thus, cluster **1** is a boron-based heterocyclic analog to the 3,5-dehydrophenyl cation, which enriches the chemical analogy between boron clusters and aromatic hydrocarbons. Our previous study on a C_s $B_4O_4^+$ cluster[33] showed a heterocyclic hexagon with double 6π/1σ aromaticity, albeit its 1σ framework is highly distorted and has rather limited delocalization.

(Figure 7)

Double 6π/2σ aromaticity in cluster **1** may be further characterized using the calculated nucleus-independent chemical shifts (NICSs).[65] The NICS data at B3LYP level are presented in Table 3. Here NICS(0) is calculated at the cluster center, whereas NICS(1) and $NICS_{zz}(1)$ are at 1 Å above it. The NICS values for cluster **1** are −14.70, −12.12, and −15.62 ppm, respectively, which are all highly negative, consistent with double π/σ aromaticity. The NICS data are also presented for D_{3h} $C_6H_3^+$, indicative of greater aromaticity as anticipated. A comparative summary of the bonding essence of cluster **1** and 3,5-dehydrophenyl cation is shown in Fig. 7.

4.3. Why heterocyclic D_{3h} $B_3S_3^+$ cluster? Comparison with Y-shaped C_{2v} B_3S_3 neutral and linear $C_{\infty v}$ $B_3O_3^+$ cluster

The D_{3h} $B_3S_3^+$ (**1**) cluster is the ultimate, simplest, free-standing boroxol-type heterocyclic

system, which minimizes the atom number down to as few as six. It appears that a positive charge is required in order to match the exact electron-counting for 6π/2σ double aromaticity. Furthermore, the type of heteroatoms from O to S is also a prerequisite for the present system. Note that $B_3O_3^{+/0/-}$ and $B_3S_3^{0/-}$ clusters[31,43] all have distinctly different structures than D_{3h} $B_3S_3^+$ (**1**). Therefore, it is of interest to elucidate why cluster **1** (and only **1**) adopts such unique geometry. Chemical bonding as presented in Sections 4.1 and 4.2 surely holds the key to understanding cluster **1**. We shall now discuss two other aspects of the system.

First, cationic $B_3S_3^+$ cluster has a well-defined potential energy surface (Fig. 2), with cluster **1** being 1.18 eV more stable than the nearest isomer at single-point CCSD(T). This is in contrast to neutral B_3S_3 cluster,[43] whose hexagonal structure **4** (C_{3v}, $^2A_1$) is only a low-lying isomer located 0.05 eV above the Y-shaped GM structure **5** (C_{2v}, $^2B_2$) (see Fig. 8(a)). As a technical note, **4** differs slightly from the previous C_3 structure;[43] the latter has one tiny imaginary frequency and coverts to C_{3v} upon optimization. Structure **5** is relevant to cationic isomer **3**. The latter also has high D_{3h} symmetry albeit with three terminal S ligands, which is located 3.01 eV above cationic GM cluster **1**. Therefore, a dramatic structural change occurs from neutral B_3S_3 to cationic $B_3S_3^+$, demonstrating an intriguing case in which every electron counts. This observation is associated to the frontier CMOs of **4** and **5**. The singly occupied HOMO (SOMO) of **5** is distributed along two B≡S terminals (47.4% from each ligand). It is locally in-plane B–S π bonding and formally out-of-phase between two B–S terminals. Overall, the SOMO is highly B–S bonding. In contrast, the SOMO of **4** is dominated by repulsion between B_3 (37.1%) and S_3 (59.8%), that is, B–S π antibonding. Clearly, the SOMO of **5** is far more advantageous than that of **4**, which helps rationalize that **5** has a substantially higher ionization potential (IP; 9.06 eV) than **4** (5.99 eV) at single-point CCSD(T). The distinct IP values lead to enhanced destabilization for isomer **3** upon electron removal and makes cluster **1** the well-defined GM structure for cation system. Basically, cluster **3** gains three localized B–S π bonds in sacrifice of a π sextet with respect to **1**. The resonance energy of the π sextet greatly benefits cluster **1**.

(Figure 8)

Second, why does D_{3h} $B_3S_3^+$ (**1**) GM cluster differ fundamentally in geometry from its isovalent GM $B_3O_3^+$ (**7**) counterpart? The latter has a linear geometry,[31] with hexagonal D_{3h} structure **6** being 2.87 eV higher in energy. We believe the key mechanism is the Coulomb repulsion. While **1** and **6** are isostructural and isovalent, the intramolecular charge transfers differ markedly (Fig. 8(b); Table 1). Quite surprisingly, the S atoms in **1** each carry a positive charge of +0.30 |e| and B centers are practically neutral (+0.04 |e|). Cluster **6** has positive B (+0.96 |e|) and negative S (–0.62 |e|) centers as anticipated. Considering the electronegativities of 2.04, 2.58, and 3.44 for B/S/O atoms, respectively, the charge distribution in **1** seems odd. To understand the issue, it is instructive to start with neutral C_{3v} B_3S_3 (**4**), which has virtually neutral B/S centers (–0.04 |e| versus +0.04 |e|), indicating highly covalent B–S bonding herein. Since the S centers in **4** participate heavily in the SOMO (by 59.8%), its corresponding cation cluster **1** naturally has positively charged S centers. The isovalent D_{3h} $B_3O_3^+$ (**6**) cluster and its neutral are dominated by ionicity. Specifically, the neutral has B (+0.72 |e|) versus O (–0.72 |e|) centers, whose SOMO contains 75.8% B component, leading thus to B (+0.96 |e|) and O (–0.62 |e|) in **6** upon electron removal. The Coulomb repulsion in cluster **6**, in particular for its B_3 centers, should substantial elevate it energetically, which results in a linear GM $B_3O_3^+$ (**7**) cluster. Interestingly, the linear $B_3S_3^+$ structure is a transition state and coverts automatically to rhombic isomer **2** upon optimization. The latter features an o-bond,[26,31] albeit not double π/σ aromaticity as in **1**. Covalent B–S bonding in the B–S binary clusters clearly favors heterocyclic structures.

4.4. Predicted electronic and vibrational properties of D_{3h} $B_3S_3^+$ cluster

To aid future experimental characterizations of D_{3h} $B_3S_3^+$ (**1**) GM cluster, we calculated its electronic and vibrational properties. The vertical electron affinity (VEA) of cluster **1** is calculated to be 6.22 and 5.74 eV at the B3LYP/6-311+G(d,p) and single-point CCSD(T) levels, respectively. The latter value is considered more reliable, which is substantially greater than that of D_{3h} $C_6H_3^+$ cluster (5.25 eV at B3LYP; 4.86 eV at single-point CCSD(T)), suggesting that

cluster **1** is a relatively stable species. Since D_{3h} $B_3S_3^+$ (**1**) cluster is closed-shell with 6π/2σ aromaticity and has a sizable energy gap between its HOMO and lowest unoccupied molecular orbital (LUMO) at B3LYP (5.03 eV; Table 1), the above VEA values are remarkable and further demonstrate the robustness of the species.

(Figure 9)

A simulated infrared (IR) spectrum of cluster **1** is shown in Fig. 9. The predominant characteristic peak at 1168 cm^{-1} and that at 364 cm^{-1} are associated to in-plane bending of B and S atoms, respectively, in the direction tangential to heterocyclic ring. Additional weak peaks at 240 and 598 cm^{-1} are due to the out-of-plane B–S bending and the B–B stretching, respectively. These peaks are vibrational signatures of cluster **1**.

5. Conclusions

In conclusion, we report on first-principles theoretical prediction of an ultimate small boroxol-type D_{3h} $B_3S_3^+$ ($^1A_1'$) cluster in the free-standing form. It has a heteroatomic hexagonal shape, being a well-defined global minimum according to computer global searches. This goal is achievable only upon minimizing the size of binary clusters to six atoms so as to eliminate any ligands, reducing valence electrons down to 26 (that is, 4 less than benzene), and substituting O with S to enhance bonding covalency. Chemical bonding in D_{3h} $B_3S_3^+$ cluster turns out to be highly covalent with no net intramolecular charge transfers from B to S. The heterocyclic cluster features 6π/2σ double aromaticity, mimicking closely the 3,5-dehydrophenyl cation species. The bonding covalency differs markedly from isovalent D_{3h} $B_3O_3^+$ cluster, whose intramolecular Coulomb repulsion strongly destabilizes its hexagonal geometry, leading to a linear global minimum. The D_{3h} $B_3S_3^+$ cluster offers an interesting example in which every electron makes a difference.

Acknowledgements

This work was supported by the National Natural Science Foundation of China (21873058 and 21573138) and the Natural Science Foundation of Shandong Province (ZR2017MB023).

H.-J.Z. also gratefully acknowledges support from the Sanjin Scholar Distinguished Professors Program.

References

[1] L. Hanley, J. L. Whitten and S. L. Anderson, *J. Phys. Chem.*, **1988**, *92*, 5803.

[2] J. E. Fowler and J. M. Ugalde, *J. Phys. Chem. A*, **2000**, *104*, 397.

[3] J. Aihara, *J. Phys. Chem. A*, **2001**, *105*, 5486.

[4] J. Aihara, H. Kanno and T. Ishida, *J. Am. Chem. Soc.*, **2005**, *127*, 13324.

[5] E. Oger, N. R. M. Crawford, R. Kelting, P. Weis, M. M. Kappes and R. Ahlrichs, *Angew. Chem., Int. Ed.*, **2007**, *46*, 8503.

[6] H. J. Zhai, A. N. Alexandrova, K. A. Birch, A. I. Boldyrev and L. S. Wang, *Angew. Chem., Int. Ed.*, **2003**, *42*, 6004.

[7] H. J. Zhai, B. Kiran, J. Li and L. S. Wang, *Nat. Mater.*, **2003**, *2*, 827.

[8] B. Kiran, S. Bulusu, H. J. Zhai, S. Yoo, X. C. Zeng and L. S. Wang, *Proc. Natl. Acad. Sci. USA*, **2005**, *102*, 961.

[9] A. N. Alexandrova, A. I. Boldyrev, H. J. Zhai and L. S. Wang, *Coord. Chem. Rev.*, **2006**, *250*, 2811.

[10] A. P. Sergeeva, D. Y. Zubarev, H. J. Zhai, A. I. Boldyrev and L. S. Wang, *J. Am. Chem. Soc.*, **2008**, *130*, 7244.

[11] W. Huang, A. P. Sergeeva, H. J. Zhai, B. B. Averkiev, L. S. Wang and A. I. Boldyrev, *Nat. Chem.*, **2010**, *2*, 202.

[12] A. P. Sergeeva, Z. A. Piazza, C. Romanescu, W. L. Li, A. I. Boldyrev and L. S. Wang, *J. Am. Chem. Soc.*, **2012**, *134*, 18065.

[13] W. L. Li, Q. Chen, W. J. Tian, H. Bai, Y. F. Zhao, H. S. Hu, J. Li, H. J. Zhai, S. D. Li and L. S. Wang, *J. Am. Chem. Soc.*, **2014**, *136*, 12257.

[14] Z. A. Piazza, H. S. Hu, W. L. Li, Y. F. Zhao, J. Li and L. S. Wang, *Nat. Commun.*, **2014**, *5*, 3113.

[15] H. J. Zhai, Y. F. Zhao, W. L. Li, Q. Chen, H. Bai, H. S. Hu, Z. A. Piazza, W. J. Tian, H. G. Lu, Y. B. Wu, Y. W. Mu, G. F. Wei, Z. P. Liu, J. Li, S. D. Li and L. S. Wang, *Nat. Chem.*, **2014**, *6*, 727.

[16] Y. J. Wang, X. Y. Zhao, Q. Chen, H. J. Zhai and S. D. Li, *Nanoscale*, **2015**, *7*, 16054.

[17] J. C. Guo, L. Y. Feng, Y. J. Wang, S. Jalife, A. Vásquez-Espinal, J. L. Cabellos, S. Pan, G. Merino

and H. J. Zhai, *Angew. Chem., Int. Ed.*, **2017**, *56*, 10174.

[18] Q. Chen, W. L. Li, Y. F. Zhao, S. Y. Zhang, H. S. Hu, H. Bai, H. R. Li, W. J. Tian, H. G. Lu, H. J. Zhai, S. D. Li, J. Li and L. S. Wang, *ACS Nano*, **2015**, *9*, 754.

[19] Q. Chen, S. Y. Zhang, H. Bai, W. J. Tian, T. Gao, H. R. Li, C. Q. Miao, Y. W. Mu, H. G. Lu, H. J. Zhai and S. D. Li, *Angew. Chem., Int. Ed.*, **2015**, *54*, 8160.

[20] Y. J. Wang, Y. F. Zhao, W. L. Li, T. Jian, Q. Chen, X. R. You, T. Ou, X. Y. Zhao, H. J. Zhai, S. D. Li, J. Li and L. S. Wang, *J. Chem. Phys.*, **2016**, *144*, 064307.

[21] A. J. Mannix, X. F. Zhou, B. Kiraly, J. D. Wood, D. Alducin, B. D. Myers, X. L. Liu, B. L. Fisher, U. Santiago, J. R. Guest, M. J. Yacaman, A. Ponce, A. R. Oganov, M. C. Hersam and N. P. Guisinger, *Science*, **2015**, *350*, 1513.

[22] B. J. Feng, J. Zhang, Q. Zhong, W. B. Li, S. Li, H. Li, P. Cheng, S. Meng, L. Chen and K. H. Wu, *Nat. Chem.*, **2016**, *8*, 563.

[23] A. v. Orden and R. J. Saykally, *Chem. Rev.*, **1998**, *98*, 2313.

[24] H. J. Zhai, Q. Chen, H. Bai, S. D. Li and L. S. Wang, *Acc. Chem. Res.*, **2014**, *47*, 2435.

[25] H. J. Zhai, Q. Chen, H. Bai, H. G. Lu, W. L. Li, S. D. Li and L. S. Wang, *J. Chem. Phys.*, **2013**, *139*, 174301.

[26] L. Y. Feng, R. Li and H. J. Zhai, *Phys. Chem. Chem. Phys.*, **2019**, *21*, 20523.

[27] R. J. Doyle, *J. Am. Chem. Soc.*, **1988**, *110*, 4120.

[28] H. J. Zhai, S. D. Li and L. S. Wang, *J. Am. Chem. Soc.*, **2007**, *129*, 9254.

[29] H. J. Zhai, C. Q. Miao, S. D. Li and L. S. Wang, *J. Phys. Chem. A*, **2010**, *114*, 12155.

[30] D. Z. Li, H. Bai, Q. Chen, H. G. Lu, H. J. Zhai and S. D. Li, *J. Chem. Phys.*, **2013**, *138*, 244304.

[31] Q. Chen, H. G. Lu, H. J. Zhai and S. D. Li, *Phys. Chem. Chem. Phys.*, **2014**, *16*, 7274.

[32] W. J. Tian, H. G. Xu, X. Y. Kong, Q. Chen, W. J. Zheng, H. J. Zhai and S. D. Li, *Phys. Chem. Chem. Phys.*, **2014**, *16*, 5129.

[33] T. Ou, W. J. Tian, X. R. You, Y. J. Wang, K. Wang and H. J. Zhai, *Phys. Chem. Chem. Phys.*, **2015**, *17*, 29697.

[34] W. J. Tian, X. R. You, D. Z. Li, T. Ou, Q. Chen, H. J. Zhai and S. D. Li, *J. Chem. Phys.*, **2015**, *143*, 064303.

[35] D. Z. Li, L. Y. Feng, L. J. Zhang, L. Pei, W. J. Tian, P. F. Li and H. J. Zhai, *J. Phys. Chem. A*, **2018**, *122*, 2297.

[36] D. Z. Li, L. Y. Feng, L. Pei, M. Z. Song, L. J. Zhang, H. Wang and H. J. Zhai, *Int. J. Quant. Chem.*, **2019**, *119*, e25907.

[37] A. Sommer, P. N. Walsh and D. White, *J. Chem. Phys.*, **1960**, *33*, 296.

[38] F. T. Greene and P. W. Gilles, *J. Am. Chem. Soc.*, **1962**, *84*, 3598.

[39] F. T. Greene and P. W. Gilles, *J. Am. Chem. Soc.*, **1964**, *86*, 3964.

[40] H. Y. Chen and P. W. Gilles, *J. Am. Chem. Soc.*, **1970**, *92*, 2309.

[41] H. Y. Chen and P. W. Gilles, *J. Phys. Chem.*, **1972**, *76*, 2035.

[42] D. Z. Li, S. G. Zhang and C. C. Dong, *Eur. J. Inorg. Chem.*, **2016**, 1103.

[43] C. C. Dong, D. Z. Li and X. D. Zheng, *J. Clust. Sci.*, **2016**, *27*, 1591.

[44] D. Z. Li, R. Li, L. J. Zhang, T. Ou and H. J. Zhai, *Phys. Chem. Chem. Phys.*, **2016**, *18*, 21412.

[45] D. Z. Li, H. Bai, T. Ou, Q. Chen, H. J. Zhai and S. D. Li, *J. Chem. Phys.*, **2015**, *142*, 014302.

[46] L. J. Zhao, X. L. Xu, H. G. Xu, G. Feng and W. J. Zheng, *New J. Chem.*, **2018**, *42*, 16021.

[47] L. J. Zhao, H. G. Xu, G. Feng, P. Wang, X. L. Xu and W. J. Zheng, *Phys. Chem. Chem. Phys.*, **2016**, *18*, 6175.

[48] G. Ferlat, T. Charpentier, A. P. Seitsonen, A. Takada, M. Lazzeri, L. Cormier, G. Calas and F. Mauri, *Phys. Rev. Lett.*, **2008**, *101*, 065504.

[49] H. Diercks and B. Krebs, *Angew. Chem., Int. Ed. Engl.*, **1977**, *16*, 313.

[50] J. Chandrasekhar, E. D. Jemmis and P. v. R. Schleyer, *Tetrahedron Lett.*, **1979**, *39*, 3707.

[51] P. v. R. Schleyer, H. Jiao, M. N. Glukhovtsev, J. Chandrasekhar and E. Kraka, *J. Am. Chem. Soc.*, **1994**, *116*, 10129.

[52] A. P. Sergeeva, B. B. Averkiev, H. J. Zhai, A. I. Boldyrev and L. S. Wang, *J. Chem. Phys.*, **2011**, *134*, 224304.

[53] M. Saunders, *J. Comput. Chem.*, **2004**, *25*, 621.

[54] P. P. Bera, K. W. Sattelmeyer, M. Saunders, H. F. Schaefer III and P. v. R. Schleyer, *J. Phys. Chem. A*, **2006**, *110*, 4287.

[55] A. D. Becke, *J. Chem. Phys.*, **1993**, *98*, 5648.

[56] C. Lee, W. Yang and R. G. Parr, *Phys. Rev. B*, **1988**, *37*, 785.

[57] M. J. Frisch, G. W. Trucks, H. B. Schlegel, G. E. Scuseria, M. A. Robb, J. R. Cheeseman, G. Scalmani, V. Barone, G. A. Petersson, H. Nakatsuji, X. Li, M. Caricato, A. V. Marenich, J. Bloino, B. G. Janesko, R. Gomperts, B. Mennucci, H. P. Hratchian, J. V. Ortiz, A. F. Izmaylov, J. L. Sonnenberg, D. Williams-Young, F. Ding, F. Lipparini, F. Egidi, J. Goings, B. Peng, A. Petrone, T. Henderson, D. Ranasinghe, V. G. Zakrzewski, J. Gao, N. Rega, G. Zheng, W. Liang, M. Hada, M. Ehara, K. Toyota, R. Fukuda, J. Hasegawa, M. Ishida, T. Nakajima, Y. Honda, O. Kitao, H. Nakai, T. Vreven, K. Throssell, J. A. Montgomery, J. E. Peralta, F. Ogliaro, M. J. Bearpark, J. J. Heyd, E. N. Brothers, K. N. Kudin, V. N. Staroverov, T. A. Keith, R. Kobayashi, J. Normand, K. Raghavachari, A. P. Rendell, J. C. Burant, S. S. Iyengar, J. Tomasi, M. Cossi, J. M. Millam, M. Klene, C. Adamo, R. Cammi, J. W. Ochterski, R. L. Martin, K. Morokuma, O. Farkas, J. B. Foresman and D. J. Fox, *Gaussian 16*, Revision A.03, Wallingford, CT, **2016**.

[58] J. P. Perdew, K. Burke and M. Ernzerhof, *Phys. Rev. Lett.*, **1996**, *77*, 3865.

[59] R. J. Bartlett and M. Musiał, *Rev. Mod. Phys.*, **2007**, *79*, 291.

[60] E. D. Glendening, J. K. Badenhoop, A. E. Reed, J. E. Carpenter, J. A. Bohmann, C. M. Morales and F. Weinhold, *NBO 5.0*, Theoretical Chemistry Institute, University of Wisconsin, Madison, WI, **2001**.

[61] D. Y. Zubarev and A. I. Boldyrev, *Phys. Chem. Chem. Phys.*, **2008**, *10*, 5207.

[62] T. Lu and F. Chen, *J. Comput. Chem.*, **2012**, *33*, 580.

[63] P. Pyykkö, *J. Phys. Chem. A*, **2015**, *119*, 2326.

[64] J. M. Millam, V. Bakken, W. Chen, W. L. Hase and H. B. Schlegel, *J. Chem. Phys.*, **1999**, *111*, 3800.

[65] P. v. R. Schleyer, C. Maerker, A. Dransfeld, H. Jiao and N. J. R. v. E. Hommes, *J. Am. Chem. Soc.*, **1996**, *118*, 6317.

Table 1. Calculated Wiberg bond indices (WBIs), natural atomic charges (q, in |e|), and HOMO–LUMO energy gap (Gap, in eV) of D_{3h} $B_3S_3^+$ (**1**) cluster at the B3LYP/6-311+G(d,p) level. Also tabulated for comparison are those of isovalent D_{3h} $B_3O_3^+$ (**6**) cluster.

Species	Bond	WBI	Atom	q	Gap
D_{3h} $B_3S_3^+$ (**1**)	B–S	1.26	B	+0.04	5.03
	B–B	0.56	S	+0.30	
D_{3h} $B_3O_3^+$ (**6**)[a]	B–O	0.99	B	+0.96	5.06
	B–B	0.49	O	–0.62	

[a] D_{3h} $B_3O_3^+$ (**6**) cluster is a highly energetic isomer.

Table 2. Composition analysis for selected canonical molecular orbitals (CMOs) of D_{3h} $B_3S_3^+$ (**1**) and D_{3h} $B_3O_3^+$ (**6**) clusters.

Species	CMO	B_3 (%)			S_3/O_3 (%)		
		p	s	total	p	s	total
D_{3h} $B_3S_3^+$	HOMO	46.2	2.1	48.3	48.6	2.1	50.7
	HOMO−1	13.2	0	13.2	86.0	0	86.0
	HOMO−1′	13.2	0	13.2	86.0	0	86.0
	HOMO−3	56.7	0	56.7	42.3	0	42.3
D_{3h} $B_3O_3^{+a}$	HOMO	50.1	0	50.1	48.6	0.6	49.2
	HOMO−1	8.0	0	8.0	91.4	0	91.4
	HOMO−1′	8.0	0	8.0	91.4	0	91.4
	HOMO−4	39.0	0	39.0	60.6	0	60.6

[a] D_{3h} $B_3O_3^+$ (**6**) cluster is a highly energetic isomer.

Table 3. Calculated nucleus-independent chemical shifts (NICSs) of D_{3h} $B_3S_3^+$ (**1**) cluster at the B3LYP/6-311+G(d,p) level, as compared to those of the corresponding hydrocarbon D_{3h} $C_6H_3^+$ ($^1A_1'$) species.

Species	NICS(0)[a]	NICS(1)[a]	$NICS_{zz}(1)$[a]
D_{3h} $B_3S_3^+$ (**1**)	−14.70	−12.12	−15.62
D_{3h} $C_6H_3^+$	−42.65	−18.83	−50.96

[a] NICS(0) values are calculated at the center of D_{3h} cluster, whereas NICS(1) and $NICS_{zz}(1)$ are at 1.0 Å above the cluster center.

Figure Captions

Figure 1. Optimized global-minimum (GM) structure of $B_3S_3^+$ cluster, D_{3h} (**1**, $^1A_1'$), at the B3LYP/6-311+G(d,p) level. (a) Structure and bond distances (in Å). The B atoms are shown in pink and S in yellow. (b) Calculated Wiberg bond indices (WBIs) from natural bond orbital (NBO) analysis.

Figure 2. Alternative optimized structures of $B_3S_3^+$ cluster at the B3LYP/6-311+G(d,p) level. Relative energies are indicated in eV at the B3LYP/6-311+G(d,p) (with zero point energy corrections), PBE0/6-311+G(d,p) (in parentheses), and single-point CCSD(T)//B3LYP/6-311+G(d,p) (in italics) levels. The B and S atoms are shown in pink and yellow, respectively. Also presented are bond distances (in Å) for isomeric structures **2** and **3**.

Figure 3. Born-Oppenheimer molecular dynamics (BOMD) simulations for D_{3h} $B_3S_3^+$ (**1**) cluster at selected temperatures of 300, 500, and 900 K. Root-mean-square deviations (RMSDs; in Å) and maximum bond distance deviations (MAXDs; in Å) are plotted against time (in ps).

Figure 4. Pictures of occupied canonical molecular orbitals (CMOs) for D_{3h} $B_3S_3^+$ (**1**) cluster. (a) Delocalized 2σ framework. (b) Delocalized π sextet. (c) Three S $3s^2$ lone-pairs. (d) Lewis 2c-2e B–S σ bonds.

Figure 5. AdNDP bonding pattern for D_{3h} $B_3S_3^+$ (**1**) cluster. Two schemes are presented for the π framework. Occupation numbers (ONs) are shown.

Figure 6. Structure and bonding of 3,5-dehydrophenyl cation D_{3h} $C_6H_3^+$ species. (a) Bond distances (in Å). (b) WBIs. (c) AdNDP bonding pattern. ONs are shown.

Figure 7. Bonding models for 6π/2σ double aromaticity in (a) D_{3h} $B_3S_3^+$ (**1**) cluster and (b) 3,5-dehydrophenyl cation.

Figure 8. Schematic energetics diagrams relevant to D_{3h} $B_3S_3^+$ (**1**) cluster. (a) Comparison with its neutral C_{3v} B_3S_3 (**4**) counterpart, as well as neutral GM C_{2v} B_3S_3 (**5**) cluster

and D_{3h} $B_3S_3^+$ (**3**) cation. Also shown are the singly occupied HOMOs (SOMOs) of **4** and **5**. (b) Comparison with isovalent GM $C_{\infty v}$ $B_3O_3^+$ (**7**) cluster and isomeric structures C_{2v} $B_3S_3^+$ (**2**) and D_{3h} $B_3O_3^+$ (**6**).

Figure 9. Simulated infrared (IR) spectrum of D_{3h} $B_3S_3^+$ (**1**) cluster.

Figure 1.

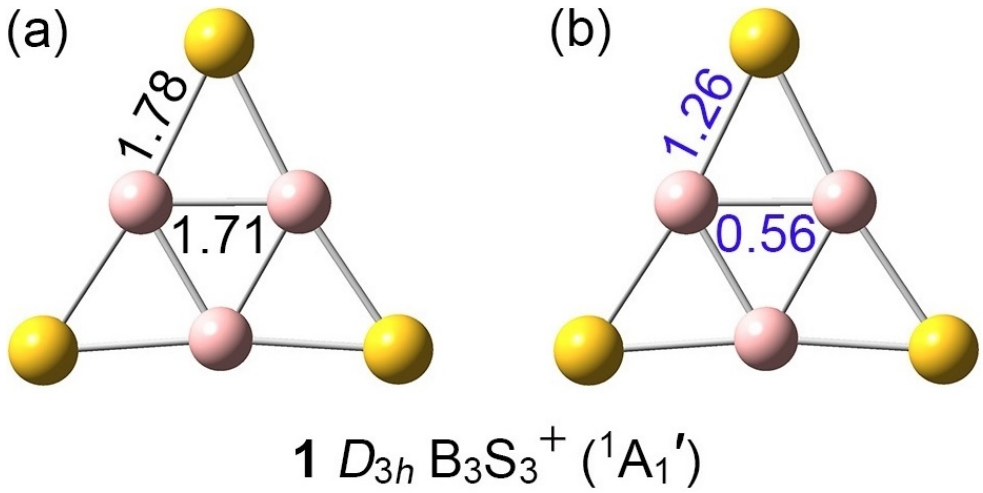

1 D_{3h} $B_3S_3^+$ ($^1A_1'$)

Figure 2.

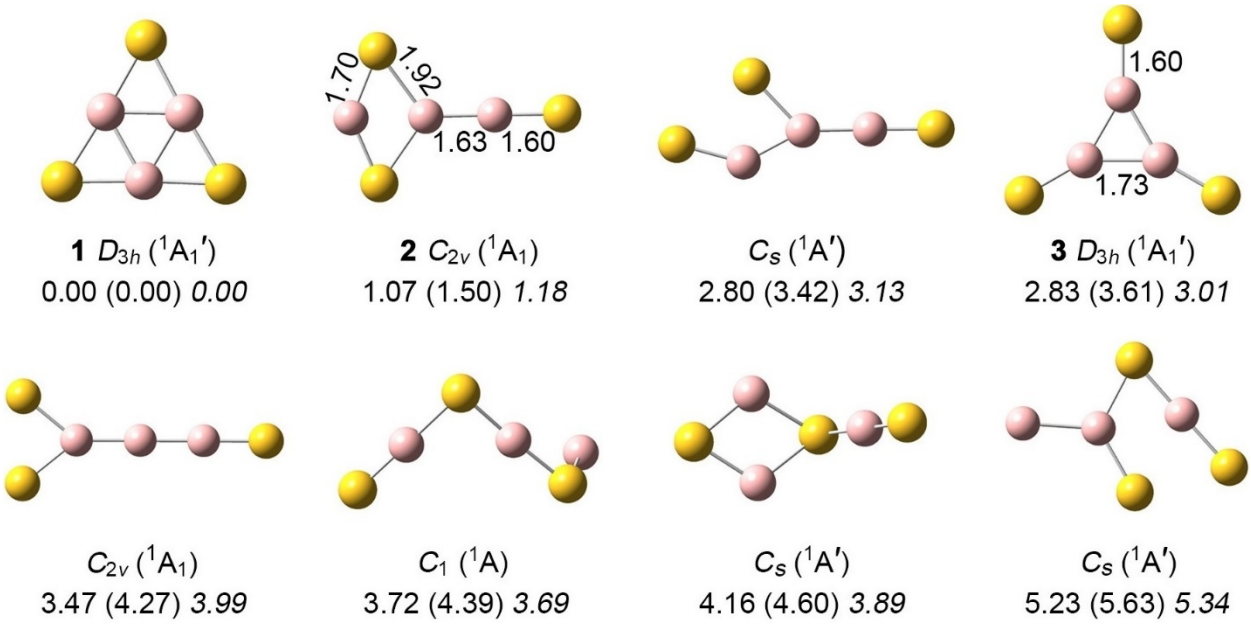

1 D_{3h} ($^1A_1'$)
0.00 (0.00) *0.00*

2 C_{2v} ($^1A_1$)
1.07 (1.50) *1.18*

C_s ($^1A'$)
2.80 (3.42) *3.13*

3 D_{3h} ($^1A_1'$)
2.83 (3.61) *3.01*

C_{2v} ($^1A_1$)
3.47 (4.27) *3.99*

C_1 (^1A)
3.72 (4.39) *3.69*

C_s ($^1A'$)
4.16 (4.60) *3.89*

C_s ($^1A'$)
5.23 (5.63) *5.34*

Figure 3.

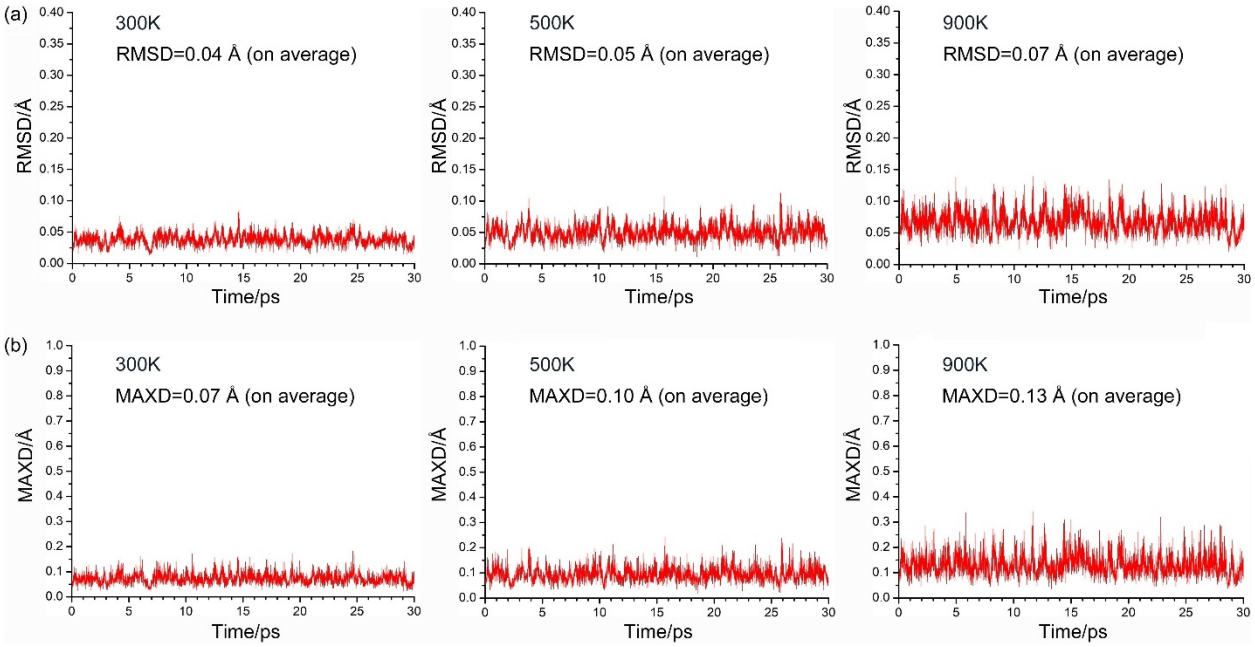
(a)
300K
RMSD=0.04 Å (on average)
500K
RMSD=0.05 Å (on average)
900K
RMSD=0.07 Å (on average)
RMSD/Å
Time/ps
(b)
300K
MAXD=0.07 Å (on average)
500K
MAXD=0.10 Å (on average)
900K
MAXD=0.13 Å (on average)
MAXD/Å
Time/ps

Figure 4.

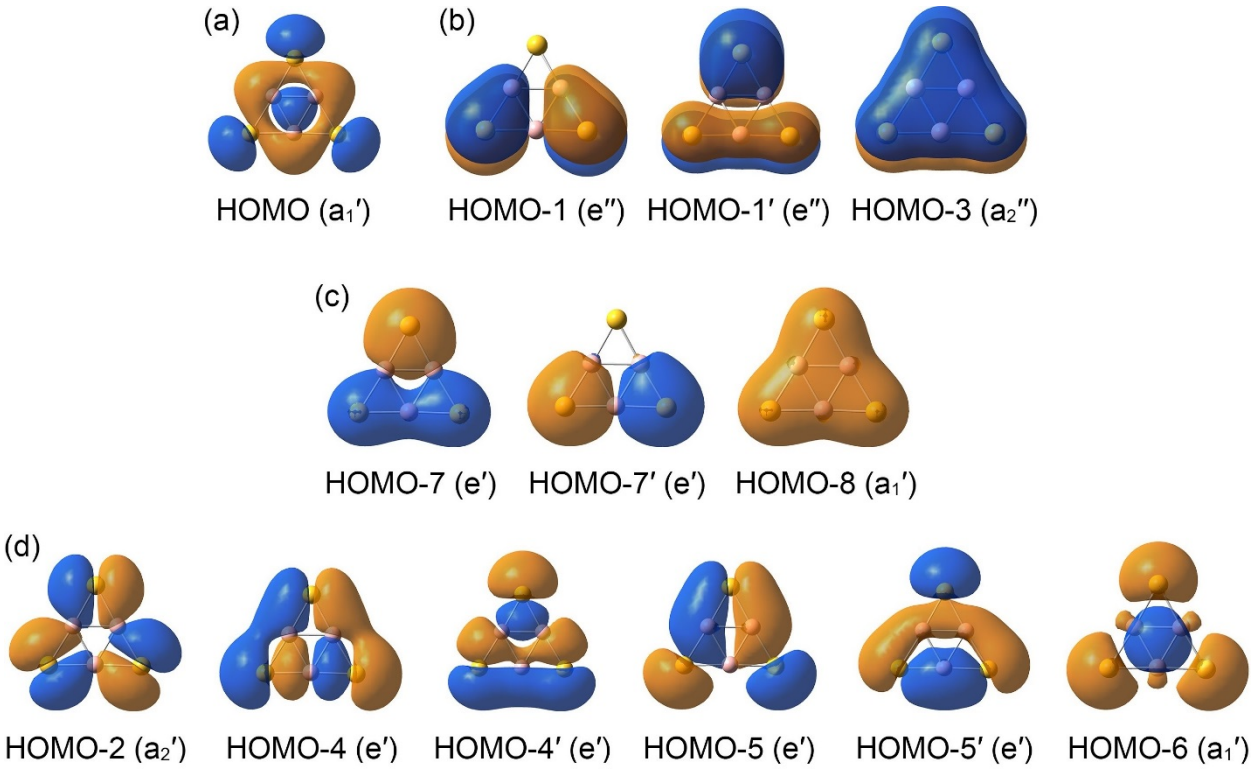
(a)
(b)
HOMO (a_1')
HOMO-1 (e'')
HOMO-1′ (e'')
HOMO-3 (a_2'')
(c)
HOMO-7 (e')
HOMO-7′ (e')
HOMO-8 (a_1')
(d)
HOMO-2 (a_2')
HOMO-4 (e')
HOMO-4′ (e')
HOMO-5 (e')
HOMO-5′ (e')
HOMO-6 (a_1')

Figure 5.

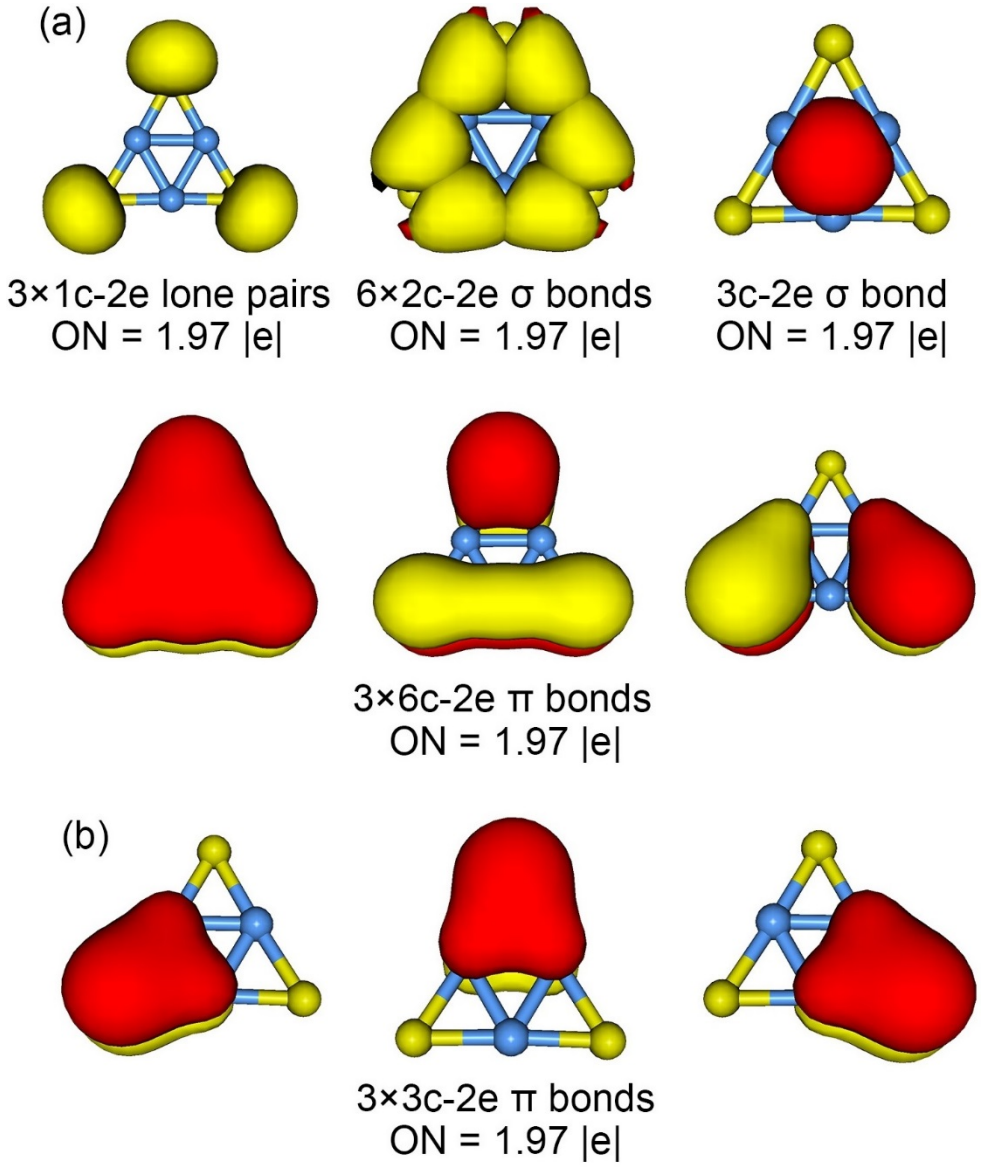
(a)
3×1c-2e lone pairs
ON = 1.97 |e|
6×2c-2e σ bonds
ON = 1.97 |e|
3c-2e σ bond
ON = 1.97 |e|
3×6c-2e π bonds
ON = 1.97 |e|
(b)
3×3c-2e π bonds
ON = 1.97 |e|

Figure 6.

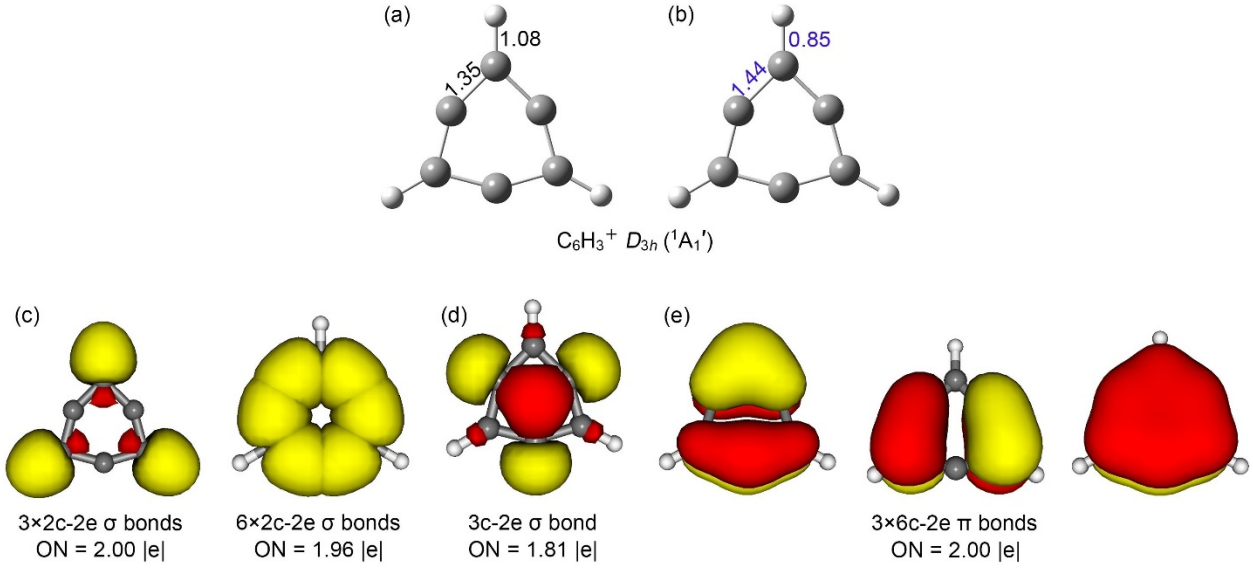
(a)
1.08
1.35
(b)
0.85
1.44
C6H3+ D3h (1A1′)
(c)
3×2c-2e σ bonds
ON = 2.00 |e|
6×2c-2e σ bonds
ON = 1.96 |e|
(d)
3c-2e σ bond
ON = 1.81 |e|
(e)
3×6c-2e π bonds
ON = 2.00 |e|

Figure 7.

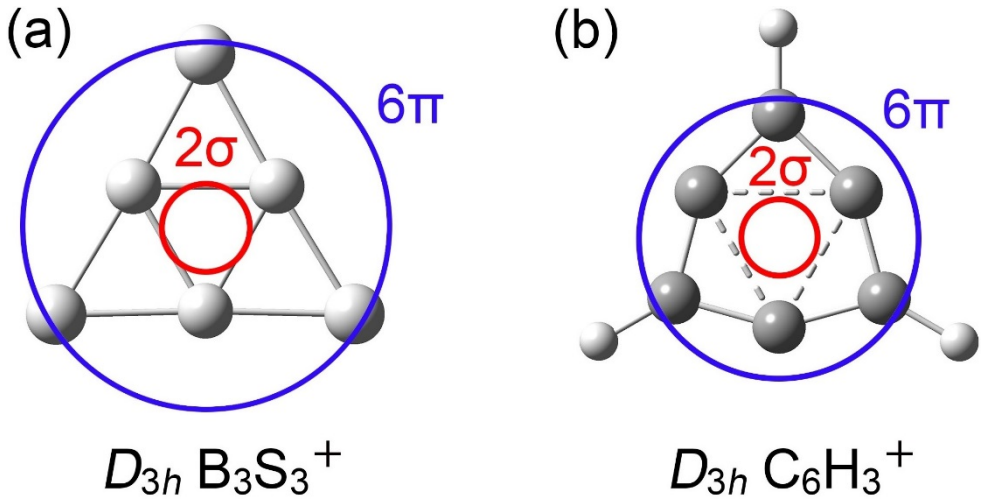

Figure 8.

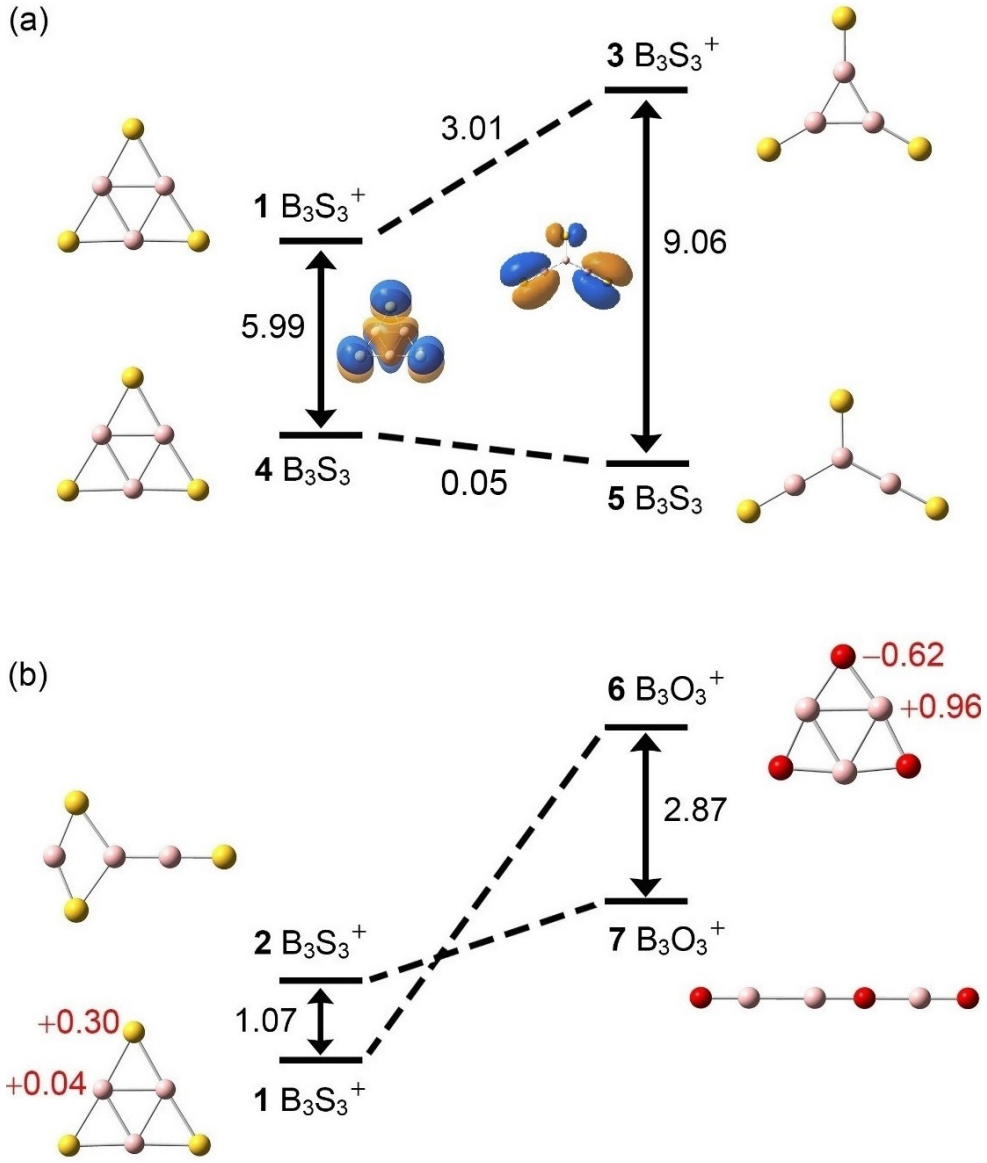
(a)
3 B3S3+
3.01
1 B3S3+
9.06
5.99
4 B3S3
0.05
5 B3S3
(b)
−0.62
+0.96
6 B3O3+
2.87
2 B3S3+
7 B3O3+
1.07
+0.30
+0.04
1 B3S3+

Figure 9.

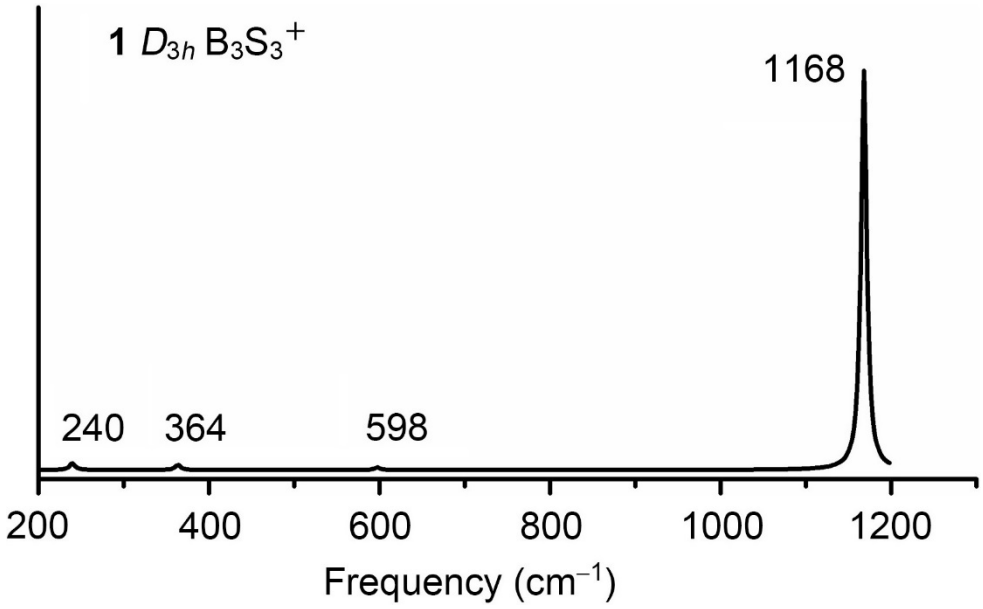
1 D_{3h} $B_3S_3^+$
1168
240
364
598
200
400
600
800
1000
1200
Frequency (cm^{-1})